NASA
Technical Memorandum 104397
AIAA 91-2022

AVSCOM
Technical Report 91-C-001

Contact Stresses in Gear Teeth—A New Method of Analysis

Paisan Somprakit and Ronald L. Huston
University of Cincinnati
Cincinnati, Ohio

and

Fred B. Oswald
Lewis Research Center
Cleveland, Ohio

Prepared for the
27th Joint Propulsion Conference
cosponsored by the AIAA, SAE, ASME, and ASEE
Sacramento, California, June 24-27, 1991

NASA

US ARMY
AVIATION
SYSTEMS COMMAND
AVIATION R&T ACTIVITY

CONTACT STRESSES IN GEAR TEETH - A NEW METHOD OF ANALYSIS

Paisan Somprakit and Ronald L. Huston
Mechanical, Industrial, and Nuclear Engineering
University of Cincinnati
Cincinnati, Ohio 45221-0072

and

Fred B. Oswald
National Aeronautics Space Administration
Lewis Research Center
Cleveland, Ohio 44135

Abstract

This paper presents a new, innovative procedure called point load superposition for determining the contact stresses in mating gear teeth. It is believed that this procedure will greatly extend both the range of applicability and the accuracy of gear contact stress analyses.

Point load superposition is based upon fundamental solutions from the theory of elasticity. It is an iterative numerical procedure which has distinct advantages over the classical Hertz method, the finite-element method (FEM), and over existing applications with the boundary element method (BEM). Specifically, friction and sliding effects, which are either excluded from or difficult to study with the classical methods, are routinely handled with the new procedure.

The paper presents the basic theory and algorithms. Several examples are presented. Results are consistent with those of the classical theories. Applications with spur gears are discussed.

Introduction

Gear tooth contact stress is the single most important factor affecting the life of a gear. Tooth contact stresses also have a significant effect upon tooth deformations and thus upon gear performance under load. However, in spite of their dominant role in gearing mechanics, contact stresses are still not well understood and they are not accurately quantified. Contact stresses are not nearly as well documented as, for example, root and fillet stresses.

One of the reasons that gear tooth contact stresses are not better understood is that the geometry and kinematics of meshing gear teeth do not satisfy the assumptions required for the application of the classical and standard Hertzion contact stress analysis.[1,2,3] The Hertz analysis assumes a contact between frictionless cylinders. It does not account for noncircular geometry such as involute geometry, and it does not include the important friction forces which occur in gear contact away from the pitch point.

Standard finite element procedures are also unsatisfactory for studying contact stresses. Contact stresses are in essence stress concentrations which are locally nonlinear. Hence, the standard finite element procedures need to be modified through the use of gap elements, large numbers of elements, and iterative procedures before they can be accurately applied in the study of contact stresses. Such modifications, although feasible,[4] are burdensome and not generally available.

A relatively new and promising procedure for contact stress analysis is the boundary element method. The boundary element method is particularly useful in regions with high stress gradients - as with contact stresses. However, this method is still under development and applications with contact stresses also require iterative procedures to obtain the contact area geometry.[5]

In this paper we present a procedure dedicated strictly to contact stress analysis with direct application in gear tooth contact stress analysis. It is similar to the boundary element method. It does not require the restrictive assumptions of the Hertz analysis. That is, with this method, noncylindrical geometry and frictional effects, as encountered in loaded meshing gears, are readily accommodated. The method is based upon the point-load superposition method developed by Paul,[6,7,8] and previous unpublished work of Sisera Jayasinghe at the University of Cincinnati.

Historically, contact stresses have been one of the most important, most widely studied, and yet most difficult problems in the theory of elasticity. Contact stress analysis can be traced back to the work of H. Hertz in 1881[1,2,3] who studied the contact deformation of smooth elastic bodies pressed together by forces normal to their contacting surfaces. He proposed that the contact region could be modeled by an elastic half space loaded over an elliptical area.

References 9 to 22 describe recent attempts to use the finite element method and the boundary element method to determine contact stresses.

The point-load superposition method presented in this paper has been outlined in a paper presented at the Health Monitoring for Propulsion Systems Conference in Cincinnati (1990).[23] The method is also documented in a recent NASA Contractor Report of the authors.[24]

The balance of the paper is divided into nine parts with the following part summarizing some preliminary results useful in the sequel. The next

three parts present the basic analysis. Numerical procedures are then discussed followed by some simple examples. The next part discusses application with spur gears. The final two parts contain a discussion and concluding remarks.

Preliminary Considerations

Consider two elastic bodies in contact. Let the contact region be divided into a mesh of elements (or cells). Let the forces transmitted across each cell be represented by a distribution of concentrated forces acting on an elastic half space. By using long-established results from the theory of elasticity, together with the principle of superposition, the stress distribution and point displacements due to a cell loading are obtained. Then, by superposing the results from each cell the resulting stress and displacement distributions within the contacting bodies may be obtained.

To develop the analysis consider an elastic half space with a concentrated normal load as in Fig. 1.

Let P be a typical point within the half space, located by the polar coordinates (r,θ) as shown. Then the radial and tangential stresses at P are:[25]

$$\sigma_{rr} = -\frac{2F}{\pi r}\cos\theta, \quad \sigma_{r\theta} = \sigma_{\theta\theta} = 0 \tag{1}$$

In rectangular coordinates, these stresses have the form:

$$\sigma_{xx} = -\frac{2F}{\pi}\frac{x^2 z}{(x^2+z^2)^2}, \quad \sigma_{zz} = -\frac{2F}{\pi} \times \frac{z^3}{(x^2+y^2)^2}, \quad \sigma_{zx} = -\frac{2F}{\pi}\frac{xz^2}{(x^2+z^2)^2} \tag{2}$$

Using the stress-strain equations and the strain-displacement equations, the displacements at a point P on the surface may be expressed as:[25]

$$u_x = -F\frac{(1-2\nu)(1+\nu)}{2E}\left(\frac{x}{|x|}\right), \qquad u_z = 2F\frac{1-\nu^2}{\pi E}\ln|h/x| \tag{3}$$

where E and ν are the elastic constant and Poisson's ratio, and where h is the distance to a reference point of zero displacement along the z-axis.

In like manner, if there is a concentrated tangential force G, the stresses at P are:[25]

$$\sigma_{rr} = -\frac{2G}{\pi r}\cos\theta, \quad \sigma_{r\theta} = \sigma_{\theta\theta} = 0 \tag{4}$$

where θ is now measured from the line of action of force G. In rectangular coordinates these stresses are

$$\sigma_{xx} = -\frac{2G}{\pi}\frac{x^3}{(x^2+z^2)^2}, \quad \sigma_{zz} = -\frac{2G}{\pi} \times \frac{xz^2}{(x^2+z^2)^2}, \quad \sigma_{zx} = -\frac{2G}{\pi}\frac{x^2 z}{(x^2+z^2)^2} \tag{5}$$

The displacement of a surface point are then

$$u_x = -2G\frac{(1-\nu^2)}{\pi E}\ln|x| + c, \qquad u_z = G\frac{(1-2\nu)(1+\nu)}{2E}\left(\frac{x}{|x|}\right) \tag{6}$$

where c is a constant determined from a zero-displacement reference point.

Next, consider an elastic half space with a distributed normal and tangential loading over a portion of the surface as depicted in Fig. 2.

Then the resulting stresses and displacements at a typical point P may be obtained by superposition (integration) of the foregoing results. Following the analysis of Johnson,[25] the stresses at P are:

$$\sigma_{xx} = -\frac{2}{\pi}\int_{-b}^{a}\{[zf(s)(x-s)^2 + g(s)(x-s)^3]/[(x-s)^2+z^2]^2\}ds$$

$$\sigma_{zz} = -\frac{2}{\pi}\int_{-b}^{a}\{[z^3 f(s) + z^2 g(s)(x-s)]/[(x-s)^2+z^2]^2\}ds$$

$$\sigma_{xz} = -\frac{2}{\pi}\int_{-b}^{a}\{[z^2 f(s)(x-s) + zg(s)(x-s)^2]/[(x-s)^2+z^2]^2\}ds \tag{7}$$

In like manner the tangential and normal displacements of a surface point are:[31]

$$u_x = -\frac{(1-2\nu)(1+\nu)}{2E}\left[\int_{-b}^{x} f(s)ds - \int_{x}^{a} f(s)ds\right] - \frac{2(1-\nu^2)}{\pi E}\int_{-b}^{a} g(s)\ln|x-s|ds + c_1$$

$$u_z = -\frac{2(1-\nu^2)}{\pi E}\int_{-b}^{a} f(s)\ln|x-s|ds + \frac{(1-2\nu)(1+\nu)}{2E}\left[\int_{-b}^{x} g(s)ds - \int_{x}^{a} g(s)ds\right] + c_2 \tag{8}$$

where c_1 and c_2 are constants to be determined from the displacement of an arbitrary reference point.

Application: Triangular Shape Loading Distribution

Equations (7) and (8) may be used to determine the effects of the force distribution in the contact region. If the region is divided into a mesh of elements (or cells), then the effects of the loadings on the individual cells may be superimposed. Moreover, the general loading in the contact region may be represented by the superimposed loadings on the cells. A triangular (that is, piecewise linear) loading distribution over a cell forms a convenient basis for modelling the general loading distribution.

The contribution of a triangular load on an individual cell to the stress at a typical point P may be obtained by letting $f(x)$ and $g(x)$ of Eqs. (7) and (8) have the forms:

$$f(x) = f_o(a-|x|)/a\ ,\ g(x) = g_o(a-|x|)/a\ ,\ |x| \leq a \tag{9}$$

where a is the half-width of the cell whose center is at the origin, and where f_o and g_o are the peak triangular normal and tangential loadings as depicted in Fig. 3.

By substituting from Eqs. (9) into (7) and by performing the indicated integrations, the resulting stresses at P (Fig. 3) are:[25]

$$\sigma_{xx} = \frac{f_o}{\pi a}[(x-a)\theta_1 + (x+a)\theta_2 - 2x\theta + 2z\ln(r_1r_2/r^2)] + \frac{g_o}{\pi a}[(2x\ln(r_1r_2/r^2) + 2a\ln(r_2/r_1) - 3z(\theta_1+\theta_2-2\theta)]$$

$$\sigma_{zz} = \frac{f_o}{\pi a}[(x-a)\theta_1 + (x+a)\theta_2 - 2x\theta] - \frac{g_o z}{\pi a}(\theta_1+\theta_2-2\theta)$$

$$\sigma_{xz} = -\frac{f_o z}{\pi a}(\theta_1+\theta_2-2\theta) + \frac{g_o}{\pi a}[(x-a)\theta_1 + (x+a)\theta_2 - 2x\theta + 2z\ln(r_1r_2r^2)] \tag{10}$$

where r_1, r_2, r, θ_1, θ_2, and θ are given by (Fig. 3):

$$r_1^2 = (x-a)^2 + z^2\ ,\ r_2^2 = (x+a)^2 + z^2,\quad r^2 = x^2 + z^2,\ \tan\theta_1 = z/(x-a),\quad \tan\theta_2 = z/(x+a),\ \tan\theta = z/x \tag{11}$$

Similarly, the displacements of a surface point are:

$$u_x = Ag_o[(x+a)^2\ell n(x/a+1)^2 + (x-a)^2\ell n(x/a-1)^2 - 2x^2\ell n(x/a)^2] + Bf_o + C_1$$

$$u_z = Af_o[(x+a)^2\ell n(x/a+1)^2 + (x-a)^2\ell n(x/a-1)^2 - 2x^2\ell n(x/a)^2] - Bg_o + C_2 \tag{12}$$

where C_1 and C_2 are constants to be determined from the displacements of a reference point and where A and B are defined as:

$$A = \frac{-(1-\nu^2)}{2\pi Ea}$$

$$B = \begin{cases} \mp\dfrac{(1-2\nu)(1+\nu)}{E}\left(\dfrac{a}{2}\right) & \text{for } x > a \\ \dfrac{-(1-2\nu)(1+\nu)x(a-|a/2|)}{Ea} & \text{for } |x| \leq a \end{cases} \tag{13}$$

Modeling of Contact Force Distribution

To illustrate how these results can be superimposed in the contact region, suppose that the contact force distribution is represented by the piecewise linear distribution, as in Fig. 4.

Let the contact region be divided into n equal-width elements (or cells) as shown. Then, just as the region is discretized so also are the force and displacement distributions. Let a be the element half-width. Then the element nodal coordinates are in multiples of a. That is, the x-coordinate of node k is:

$$x_k = ka \tag{14}$$

Let u_{ix} and u_{iz} represent the tangential and normal displacements of node i due to a triangular normal load centered at node j. Then from Eq. (12), u_{ix} and u_{iz} may be expressed as

$$u_{ix} = -\frac{(1-2\nu)(1+\nu)}{E}d_{ij}f_j\ ,\quad u_{iz} = \left(\frac{1-\nu^2}{E}\right)c_{ij}f_j \tag{15}$$

$$c_{ij} = \begin{cases} -\dfrac{a}{2\pi}[(k+1)^2\ln(k+1)^2 + (k-1)^2\ln(k-1)^2 - 2k^2\ln k^2] & |k|>1 \\ 0 & k=0 \\ -\dfrac{2a}{\pi}\ell n4 & k=\pm 1 \end{cases} \tag{16}$$

$$d_{ij} = \begin{cases} a/2, & k>0 \\ -a/2, & k<0 \\ 0, & k=0 \end{cases}$$

where k is defined as:

$$k = i - j \tag{17}$$

Equation (15) may be used to obtain the displacements at node i due to a set of superposed triangular load distributions centered at each of the nodes. In this case the terms $c_{ij}f_i$ and $d_{if}f_j$ are interpreted as sums over j.

Finally, if there is a horizontal or tangential loading, an analogous analysis leads to displacements at node i as:

$$u_{ix} = (\frac{1-\nu^2}{E})c_{ij}g_j \ , \ u_{iz} = \frac{(1-2\nu)(1+\nu)}{E} d_{ij}g_j \qquad (18)$$

where the coefficients c_{ij} and d_{ij} are the same as those of Eq. (16) and where there is a sum on j from 1 to n.

The displacements of Eqs. (15) and (18) are measured relating to a convenient reference point, say the origin of the coordinate axes.

Contact Analysis

Equations (15) and (18) may be used to develop an iterative procedure for obtaining a detailed and comprehensive analysis of contact stresses and deformations.

To illustrate this consider two cylinders pressed together as in Fig. 5. As the cylinders are brought together they initially have line contact. Then as they are pressed tighter the line contact develops into a contact strip.

Figure 6 depicts the contact region after a finite deformation. The solid curves represent the deformed surface profiles, and the dashed curves represent the undeformed, or original profiles.

Consider two points Q_1 and Q_2 relatively distant from the contact region. Then during the compression Q_1 and Q_2 move toward the contact region and toward each other through the displacements d_{1z} and d_{2z} respectively.

Consider two typical matching surface points P_1 and P_2 separated by a distance h(x). Then as the deformation proceeds, P_1 and P_2 simultaneously move toward each other and deform inward into their respective cylinders. Let U_{1z} and U_{2z} (measured as positive <u>into</u> the respective cylinders) represent the z-axis displacements of P_1 and P_2 toward Q_1 and Q_2. Then if P_1 and P_2 come into contact, we have

$$U_{1z} + U_{2z} + h(x) = d_{1z} + d_{2z} = D_z \qquad (19)$$

where D_z is the global compressive displacement of the cylinders. If P_1 and P_2 are outside the contact region we have

$$U_{1z} + U_{2z} + h(x) > D_z \qquad (20)$$

Equations (19) and (20) can be used to determine the extent of the contact region.

If there is no relative horizontal displacement of P_1 and P_2, we have the no-slip condition

$$U_{1x} = U_{2x} \qquad (21)$$

When the cylinders are subjected to tangential loading in addition to the normal loading, the deformation geometry depends upon the relative magnitudes of the normal and tangential loads. The tangential loading causes an asymmetric deformation pattern. This asymmetry, or distortion is limited by the friction coefficient so that alternatively sliding occurs.

Figure 7 depicts the cylinders in contact with tangential loading. As before P_1 and P_2 are matching surface points at the initiation of contact. When the tangential load G is applied the distant points Q_1 and Q_2 have rigid body displacements d_{1x} and d_{2x} relative to O. If the displacements of P_1 and P_2 relative to O are denoted by S_{1x} and S_{2x}, the slip S_x between P_1 and P_2 may be defined as:

$$\begin{aligned} S_x = S_{1x} - S_{2x} &= (U_{1x} - d_{1x}) - (U_{2x} - d_{2x}) \\ &= (U_{1x} - U_{2x}) - (d_{1x} - d_{2x}) \end{aligned} \qquad (22)$$

If P_1 and P_2 are in the nonslip (stick) region s_x is zero, and then

$$U_{1x} - U_{2x} = d_{1x} - d_{2x} = D_x \qquad (23)$$

where D_x is the global tangential displacement of the cylinders.

Numerical Procedures

Equations (15) and (18), together with the constraint equations of the foregoing part, may be used to determine the nodal normal and tangential forces f_i and g_i. A difficulty which arises however, is that the extent of the contact region is not known a-priori. Hence, an iterative procedure needs to be developed which will determine the contact region as well as the nodal forces.

For the development of this procedure, it is convenient to superimpose Eqs. (15) and (18) and express them in the form:

$$u_{0x} - u_{ix} = \frac{(1-2\nu)(1+\nu)}{E} \hat{d}_{ij}f_j - \frac{1-\nu}{E}\hat{c}_{ij}g_j \qquad (24)$$

and

$$u_{0z} - u_{iz} = -\frac{(1-2\nu)(1+\nu)}{E} \hat{d}_{ij}g_j - \frac{(1-\nu^2)}{E}\hat{c}_{ij}f_j \qquad (25)$$

where $\hat{c}_{oj}$ and $\hat{d}_{ij}$ are defined as

$$\hat{c}_{ij} = c_{ij} - c_{oj} \text{ and } \hat{d}_{ij} = d_{ij} - d_{oj} \qquad (26)$$

where $\hat{c}_{oj}$ and d_{oj} are influence coefficients of the origin (Eqs. (16) and (17)). Then by substituting from Eqs. (24) and (25) into Eq. (20) we have

$$\lambda_1\hat{c}_{ij}f_j + \lambda_2\hat{d}_{ij}g_j = -b_i \quad i,j = 0,\ldots,\pm n \qquad (27)$$

where

$$\lambda_1 = \frac{(1-\nu_1^2)}{E_1} + \frac{(1-\nu_2^2)}{E_2} \text{ and } \lambda_2 = \frac{(1-2\nu_1)(1+\nu_1)}{E_1} - \frac{(1-2\nu_2)(1+\nu_2)}{E_2} \qquad (28)$$

with E_1, ν_1, E_2, and ν_2 being the elastic constants of Bodies 1 and 2.

Similarly, for those nodes in the stick region Eqs. (24) and (25) together with Eq. (21) lead to

$$\lambda_3 \hat{d}_{ij} f_j - \lambda_4 \hat{c}_{ij} g_j = 0 \qquad (29)$$
$$i=1,\ldots,m;\ j=0,\ldots,\pm n$$

$$\lambda_3 = \frac{(1-2\nu_1)(1+\nu_1)}{E_1} - \frac{(1-2\nu_2)(1+\nu_2)}{E_2} \qquad (30)$$
$$\text{and } \lambda_4 = \frac{(1-\nu_1^2)}{E_1} + \frac{(1-\nu_2^2)}{E_2}$$

Finally, for those nodes in the slip region we have

$$g_i = \pm \mu f_i \quad i = -n,\ldots,p,p+m,\ldots,n \qquad (31)$$

where the sign is chosen so that the force direction is opposite to the direction of slip.

In Eqs. (27), (29), and (31) there are $2n + 1$ unknown f_i and $2n+1$ unknown g_i $(i = 0,\ldots,\pm n)$--that is $4n + 2$ equation. Equations (27), (29), and (31) constitute $4n + 2$ equations. However, the system is not complete since when i is zero, Eqs. (27) and (29) are degenerate. Hence, two additional equations are needed. These are obtained from global force summation leading to:

$$F = f_i A_i \text{ and } G = g_i A_i \qquad (32)$$

where A_i is the element area associated with node i.

The numerical procedure is then:

(1) Assume a contact region
(2) Divide the contact region into elements or cells
(3) Assume a stick region within the contact region
(4) Solve Eqs. (27), (29), and (31) for the nodal forces
(5) Adjust the extent of the contact region by deleting nodes with negative normal forces
(6) Adjust the stick region using Eq. (31)
(7) Repeat steps (1) to (6) until convergence is obtained

This procedure is dependent upon superposing the forces from the nodes in the contact region. Therefore, the method is called point load superposition.

Example Solutions

To illustrate the efficacy of the method we first considered two frictionless, steel cylinders pressed together with a force of 1000 lb per unit axial length and no tangential loading. The cylinders had radii: 100 and 150 in; elastic modulus: 30×10^6 lb/in^2; and Poisson ratio: 0.3. The cylinder surfaces were taken to be frictionless so that a comparison could be made with the classical Hertz solution, which assumes frictionless contact.

Table 1 shows a comparison of numerical results and the Hertz solution.

Next to examine the effects of friction (and hence, the consequences of neglecting friction), we considered two unlubricated cylinders with radii 100 and 150 in. made of steel and aluminum respectively. Different materials were chosen to illustrate the effects of material properties on the solutions. (The Hertz solution is based upon identical material properties of the contacting bodies.) As in the first example, the cylinders were pressed together with a normal force of 1000 lb per unit axial length. The elastic moduli for steel and aluminum were taken as: 30×10^6 and 12×10^6 lb/in.^{2} and the Poisson ratios as: 0.3 and 0.33 respectively. The friction coefficient was assigned as: 0.5 to simulate the unlubricated surfaces. Table 2 shows a comparison of numerical results and the Hertz solution. Figure 8 depicts the loading distribution in the contact region.

Finally, to examine the effects of sliding, the steel/aluminum cylinders of the previous example were also loaded tangentially to produce sliding. Table 3 shows a comparison of the numerical results and the Hertzian solution.

Figure 9 shows the normal pressure distribution obtained from the Hertz and numerical solutions. (Observe the shift in the numerical distribution due to the sliding.) Figures 10 and 11 show the shear stress distributions on the steel and aluminum cylinders for the Hertz, friction and sliding cases.

Application with Involute Spur Gears

To study contact stresses in mating gear teeth we model the teeth as contacting cylinders as depicted in Figure 12. The radii of the cylinders depends upon the position of the contact point along the line of contact.

In Fig. 12 C_1 and C_2 are the centers of the meshing gears and P is the pitch point. I_1, I_2, O_1, O_2, P, and O are points along the pressure line which is tangent to the base circles of the gears as shown. I_1 and I_2 are at the intersections of the pressure line and lines perpendicular to the pressure line passing through C_1 and C_2 respectively. O_1 and O_2 are at the intersections of the pressure line and the addenda of the gears. O is a typical contact point along the pressure line.

Then the base, pitch, and addenda circle radii are given by

$$r_{b1} = |\overline{C_1 I_1}|\ ,\ r_{b2} = |\overline{C_2 I_2}|\ ,\ r_{p1} = |\overline{C_1 P}|\ ,$$
$$r_{p2} = |\overline{C_2 P}|\ ,\ r_{a1} = |\overline{C_1 O_1}|\ ,\ r_{a2} = |\overline{C_2 O_2}| \qquad (33)$$

where the subscripts 1 and 2 identify the associated gear, and the notation $|\overline{C_1 I_1}|$ for example, designates the length of the line segment between C_1 and I_1.

Since these radii are known for a given pair of meshing gears, it is convenient to express the tooth curvatures (and hence, the contacting cylinder curvatures) in terms of these radii. From the properties of the involute profile, the tooth radii of curvature at the contact point are simply the distances from the contact point to I_1 and I_2 respectively.

Consider the following contact positions:

1. Contact at the Pitch Point

In this case the radii of curvature of the mating tooth surfaces are:

$$\rho_1 = |\overline{I_1 P}| = [\,|\overline{C_1 P}|^2 - |\overline{C_1 I_1}|^2\,]^{1/2} = \sqrt{r_{p1}^2 - r_{b1}^2} \tag{34}$$

and

$$\rho_2 = |\overline{I_2 P}| = [\,|\overline{C_2 P}|^2 - |\overline{C_2 I_2}|^2\,]^{1/2} = \sqrt{r_{p2}^2 - r_{b2}^2} \tag{35}$$

where the subscripts 1 and 2 identify the associated gear.

2. Contact on the Addendum Circle of Gear 1

In this case the radii of curvature are:

$$\rho_1 = |\overline{I_1 O_1}| = [\,|\overline{C_1 O_1}|^2 - |\overline{C_1 I_1}|^2\,]^{1/2} = \sqrt{r_{a1}^2 - r_{b1}^2} \tag{36}$$

$$\rho_2 = |\overline{I_2 O_1}| = |\overline{I_1 I_2}| - |\overline{I_1 O_1}| = (r_{p1} + r_{p2})\sin\phi - \rho_1 \tag{37}$$

where ϕ is the pressure angle.

3. Contact on the Addendum Circle of Gear 2

In this case the radii of curvature are:

$$\rho_2 = |\overline{I_2 O_2}| = [\,|\overline{C_2 O_2}|^2 - |\overline{C_2 I_2}|^2\,]^{1/2} = \sqrt{r_{a2}^2 - r_{b2}^2} \tag{38}$$

and

$$\rho_1 = |\overline{I_1 I_2}| - |\overline{I_2 O_2}| = (r_{p1} + r_{p2})\sin\phi - \rho_2 \tag{39}$$

4. Contact at Other Points

Cases 2 and 3 are at the contact extremes with Case 1 being intermediate. For some other contact point, the radii of curvature will be different than these cases, but it can be calculated using the same procedures as in the above cases.

The developed numerical procedures may now be used to calculate the contact stresses on the mating teeth. To illustrate this application, consider two identical spur gears in mesh with the following properties.

Number of teeth	18
Pitch diameter	3.5433 in.
Face width	0.3937 in.
Pressure angle	20°
Transmitted load (tangential)	808 lb
Elastic modulus	30×10^6 psi
Poisson ratio	0.3

The calculated maximum contact stress and maximum shear (Von Mises) stress for two different contact points are presented in Table 4. The high contact stress at the surface is primarily hydrostatic loading and does not normally produce failure. The maximum sheer stress which occurs beneath the surface can initiate crack formation which leads to pitting fatigue failure.

Discussion

The method employs a double discretation: one of the contact region, the other of the force distribution. The execution of the method involves an iterative procedure to determine the extent of the contact region. In this way the method is clearly more laborious than the classical Hertz method and even elementary finite-element methods (FEM). In exchange, however, the method is believed to provide a more accurate and comprehensive analysis than either the Hertz or FEM techniques.

Although these examples employ bodies with simple geometries (cylinders), the method outlined herein is not restricted to simple geometries. Indeed, there are no restrictions on the geometry so long as the contacting surfaces are continuous and geometrically smooth (that is, with continuous derivatives).

The examples demonstrate the efficacy of the method. They show that the numerical results are extremely close to those of the classical Hertz solutions, for those cases where the Hertz solution is applicable. Indeed, the stresses are virtually identical whereas there is a slight difference in the geometric results - that is, the contact region width and the location of the maximum shear stress. (The Hertz solution assumes frictionless static contact between identical materials.)

The second and third example demonstrate the significant effects of friction and sliding in contact analysis. The examples also show that the softer material has lesser stress.

In addition it is seen that friction and sliding significantly increase the shear stresses. Indeed, when there is sliding with a relatively high friction coefficient, the maximum shear stress occurs on the surface as opposed to being beneath the surface (Figs. 10 and 11).

The conditions of gear tooth contact (Non-cylindrical surface, friction, and sliding) do not satisfy the assumptions for Hertz theory. The point load superposition method is not restricted by these assumptions. The gear stress results of Table 4 are believed to be accurate, limited only by the precision of the descretation.

The method outlined herein is developed for a two-dimensional analysis with a triangular load on the individual elements or cells. The triangular load provides for a piecewise linear representation of the contact loading. The method can be extended to higher order load representations (for example, the use of cubic splines) and to three-dimensional analysis.

Conclusions

A point load superposition procedure based on the theory of elasticity has been used to study contact stresses between elastic bodies, including meshing spur gear teeth. This method is validated by comparison with results from the classical Hertz method for frictionless cylinders in contact. The following specific conclusions are reached:

1. A new method of contact stress analysis has been presented. It is a numerical method which has fewer restrictions than classical procedures.

2. The method is applicable for a broad range of geometries of the contacting bodies. The contacting bodies may have different material properties. The contacting surfaces need not be smooth. Sliding between the contacting surfaces is also permitted.

3. The accuracy of the method is demonstrated by a comparison with results from classical methods for simple cases where the classical method is applicable.

4. The established efficacy of the method justifies applications with contacting gear teeth.

Acknowledgment

The research for the analysis of this paper was partially supported by a grant from the National Aeronautics and Space Administration to the University of Cincinnati. (Grant No. NSG 3188)

References

1. H. Hertz, "On the Contact of Elastic Solids" (in German), J. Reine und Angwandte Mathematik, Vol. 92, 1882, pp 156-171. (See [3] for English translation).

2. H. Hertz, "On the Contact of Rigid Elastic Solids and an Hardness" (in German), Verhandlungen des Vereins zur Beforderung des Gewerbefleisses, Leipzig, 1882.

3. D.E. Jones and G.A. Schott, H. Hertz, Miscellaneous Papers, Macmillan and Co., London, 1896.

4. C.-M. Hseih, "Contact Stresses of Meshing Spur Gear Teeth: Use of Incremental Finite Element Techniques," Ph.D. Dissertation, University of Cincinnati, 1990.

5. H.-C. Sun, "Use of the Boundary Element Method in Contact Stress Analysis," Ph.D. Dissertation, University of Cincinnati, 1989.

6. C. Liu and B. Paul, "Rolling Contact With Friction and Non-Hertzian Pressure Distribution," Journal of Applied Mechanics, Vol. 56, 1989, pp. 814-820.

7. B. Paul and J. Hashemi, "Contact Pressure on Closely Conforming Elastic Bodies, Journal of Applied Mechanics, Vol. 48, 1981, p 543.

8. K.P. Singh and B. Paul, "Numerical Solution on Non-Hertzian Elastic Contact Problems," Journal of Applied Mechanics, vol. 41, 174, pp. 484-490.

9. W.H. Chen and J.T. Yel, "Three-Dimensional Finite Element Analysis of Static and Dynamic Contact Problems With Friction, Computers and Structures, Vol. 35, No. 5, 1990, pp. 541-542.

10. N. Chandrasekaraw, W.E. Haisler, and R.E. Goforth, "A Solution Method for Planar and Axisymmetric Contact Problems," International Journal of Numerical Methods in Engineering, Vol. 21, 1985, pp 65-88.

11. K.J. Bathe and A. Chandary, "A Solution Method for Planar and Axisymmetric Contact Problems," International Journal of Numerical Methods in Engineering, Vol. 21, 1985, pp. 65-68.

12. M.U. Rahman, R.E. Rowlands, and R.D. Cook, "An Iterative Procedure for Finite Element Stress Analysis of Frictional Contact Problems," Computers and Structures, Vol. 14, 1984, pp. 947-954.

13. T.D. Sachdeva and C.V. Ramakrishnan, "A Finite Element Solution for the Two-Dimensional Elastic Contact Problems with Friction," International Journal of Numerical Methods in Engineering, Vol. 17, 1981, pp. 1257-1271.

14. R.J. Gu, "Moving Finite Element Analysis for Two-Dimensional Frictionless Contact Problems, Computers and Structures, Vol. 33, No. 2, 1989, pp. 543-549.

15. H.S. Jing and M.-L. Liao, "An Improved Finite Element Scheme for Elastic Contact Problems with Friction," Computers and Structures, Vol. 35, No. 5, 1990, pp. 571-578.

16. N. Akamato and M. Nakazawa, "Finite Element Increment Contact Analysis with Various Frictional Conditions," International Journal of Numerical Methods in Engineering, Vol. 14, 1979, pp. 337-357.

17. M. Mazurkiewicz and W. Ostachowicz, "Theory of the Finite Element Method for Elastic Contact Problems of Solid Bodies," Computer and Structures, Vol. 17, 1983, pp. 51-59.

18. K.P. Oh and S.M. Rohde, "Numerical Solution of the Point Contact Problem Using the Finite Element Method," International Journal for Numerical Methods in Engineering, Vol. 11, 1977, pp. 1507-1578.

19. W. Ostachowicz, "Mixed Finite Element Method for Contact Problems," Computers and Structures, Vol. 18, 1984, pp. 937-945.

20. M.J. Abdul-Mihein, A.A. Baker, and A.P. Parker, "A Boundary Integral Equation Method for Axisymmetric Elastic Contact Problems," Computers and Structures, Vol. 23, 1986, pp. 787-793.

21. T. Anderson and B.G.A. Person, "The Boundary Element Method Applied to Two-Dimensional Contact Problems," Progress in Boundary Elements, (C.A. Brebbia, Ed.) Vol. II, Chapter 5, PentechPress, London, 1982.

22. H. Sun and R.L. Huston, "An Automatic Incrementation Technique of the Boundary Element Method for Two-Dimensional Contact Problems with Friction," Computational Engineering with Boundary Elements (A.H.D. Cheng, C.A. Brebbia, and S. Grilli, Eds.) Computational Mechanics Publication, Boston, 1990, pp. 19-35.

23. P. Somprakit, R.L. Huston, and J.E. Wade, II, "Monitoring of Contact Stresses in Advanced Propulsion Systems," Proceedings of the Second Annual Health Monitoring for Space Propulsion Systems Conference, Cincinnati, Ohio, 1991, pp. 334-360.

24. P. Somprakit and R.L. Huston, "A New Procedure for Calculating Contact-Stresses in Gear Teeth," NASA CR 187094, 1991.

25. K.L. Johnson, Contact Mechanics, Cambridge, London, 1985.

Table 1. - Comparison of Hertz and Numerical Solutions for Contacting Steel Cylinders without Friction

Item	Hertz Solution	Numerical Solution	Difference
Width of Contact Region (in.)	0.136156	0.137287	0.83%
Maximum Normal Pressure (psi)	9351.35	9358.90	0.08%
Maximum Shear Stress (psi)	2808.05	2810.26	0.08%
Location of Maximum Shear on Z-Axis (in.)	0.05310	0.05352	0.79%

Table 2. - Comparison of Hertz Solutions (Identical, Frictionless Materials) and Numerical Solutions for Contacting Steel/Aluminum Cylinders with Friction (The numbers in parenthesis refer to the aluminum cylinder)

Item	Hertz Solution	Numerical Solution	Difference
Width of Contact Region (in.)	0.18896	0.18873	0.12%
Maximum Normal Pressure (psi)	6738.12	6810.89	1.08%
Maximum Shear Stress (psi)	2021.43	2081.32 (2031.28)	2.95% (0.48%)
Location of Maximum Shear on Z-Axis (in.)	0.07369	0.07967 (0.06461)	8.1% (13%)

Table 3. - Comparison of Hertz Solutions (No Sliding) and Numerical Solutions for Contacting/Sliding, Steel/Aluminum Cylinders

Item	Hertz Solution	Numerical Solution	Difference
Width of Contact Region (in.)	0.18896	0.19041	0.77%
Maximum Normal Pressure (psi)	6738.12	6737.87	0.00%
Maximum Shear Stress (psi)	2021.43	3365.39	66.4%
Location of Maximum Shear on Z-Axis (in.)	0.07369	0.00	100%
Shift of Center (in.)	0.00	0.01123	100%

Table 4. - Gear Tooth Stress Results and Comparisons

	Pitch Point Contact	Addendum Contact
Surface Contact Stress (psi)	194,480	286,013
Maximum Shear Stress (psi)	58,407	85,899
Depth to Maximium Shear Stress (in.)	0.0056	0.0038

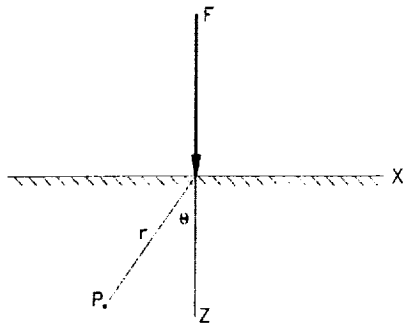

Figure 1. A Concentrated Normal Force on an Elastic Half Space

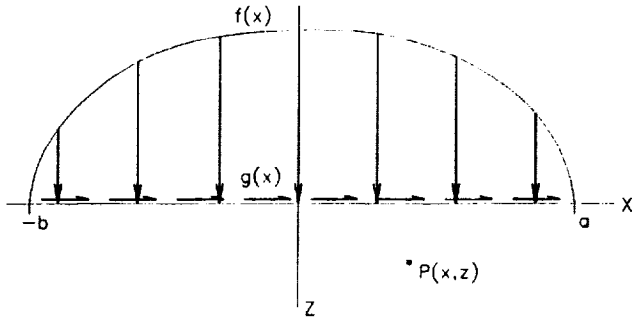

Figure 2. Elastic Half-Space with a Normal and Tangential Loading Distribution

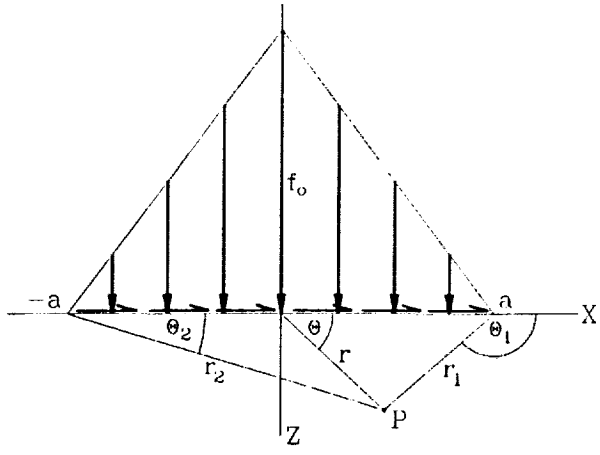

Figure 3. Triangular Normal and Tangential Loading on a Typical Cell

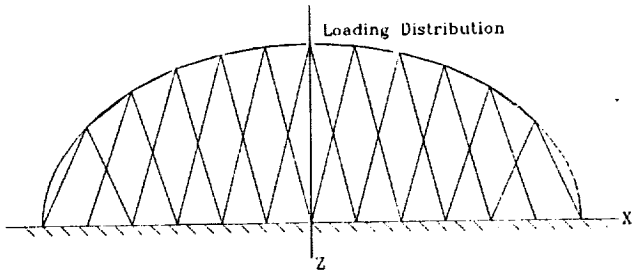

Figure 4. A Piecewise Linear Representation of a Force Distribution

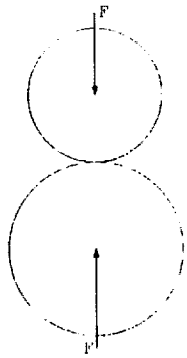

Figure 5. Two Elastic Cylinders Being Pressed Together

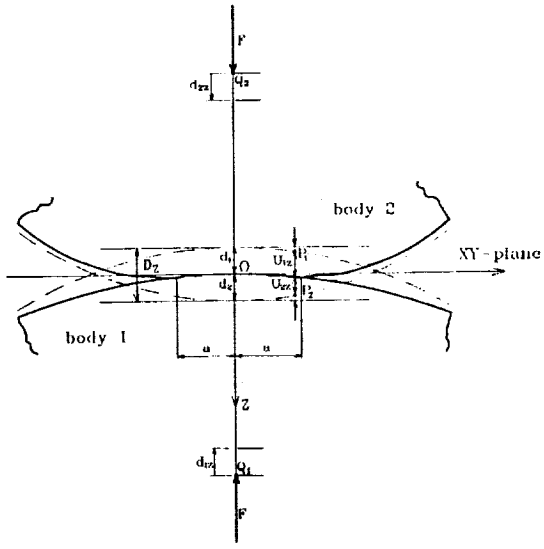

Figure 6. Contact Region of Deformed Cylinders

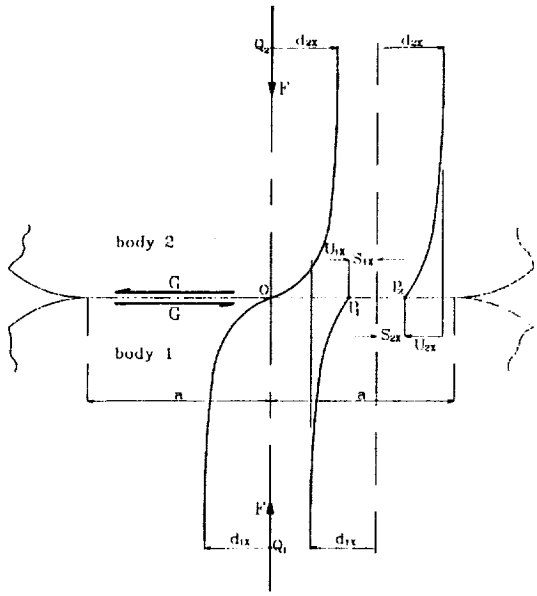

Figure 7. Contact Region with Tangential Loading

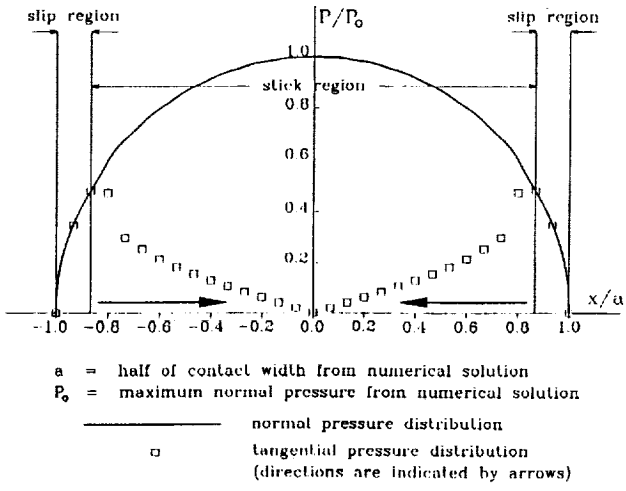

Figure 8. Contact Region Loading Distribution for Contacting Steel/Aluminum Cylinders With Friction

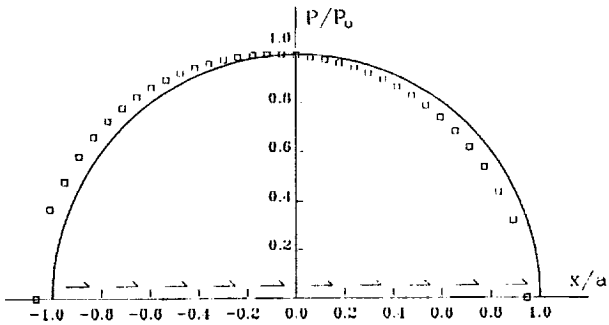

a = half of contact width from Hertzian contact
P_0 = maximum normal pressure from Hertzian contact
sliding contact
Hertzian contact

Figure 9. Comparison of Hertz and Numerical Solutions for Normal Pressure for Contacting/Sliding, Steel/Aluminum Cylinders

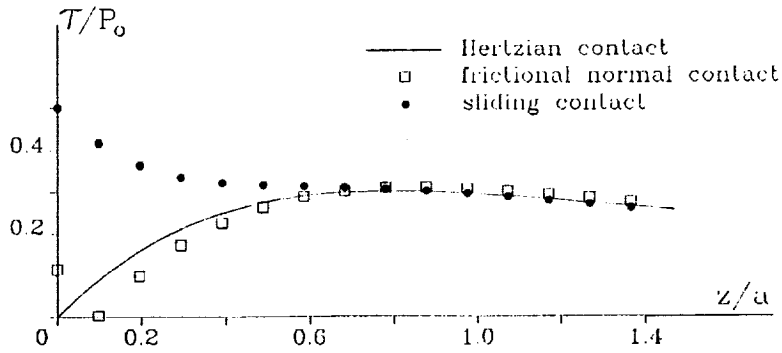

T maximum shear stress
P_0 maximum normal pressure (Hertz)
a half of contact width (Hertz)

Figure 10. Shear Stress Distributions on the Steel Cylinder.

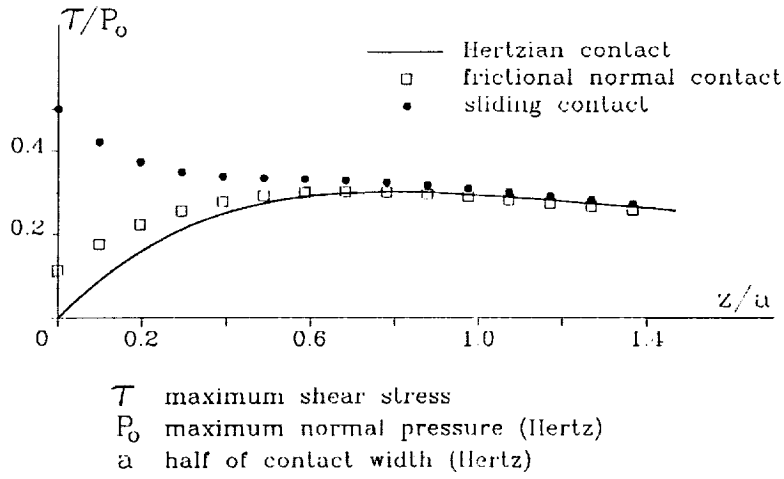

Figure 11. Shear Stress Distributions on the Aluminum Cylinder

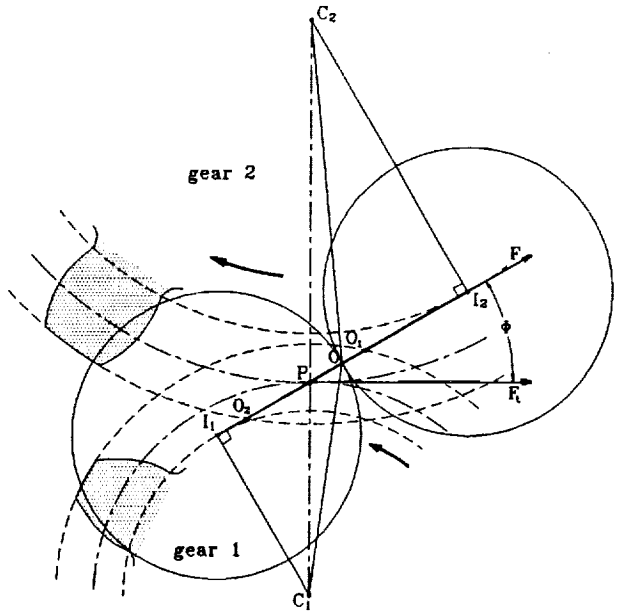

Figure 12. Modeling Mating Gear Teeth as Contacting Cylinders

NASA
National Aeronautics and Space Administration

Report Documentation Page

1. Report No.	2. Government Accession No.	3. Recipient's Catalog No.
NASA TM -104397 AVSCOM TR 91-C-001; AIAA-91-2022		

4. Title and Subtitle
Contact Stresses in Gear Teeth—A New Method of Analysis

5. Report Date

6. Performing Organization Code

7. Author(s)
Paisan Somprakit, Ronald L. Huston, and Fred B. Oswald

8. Performing Organization Report No.
E -6214

9. Performing Organization Name and Address
NASA Lewis Research Center
Cleveland, Ohio 44135 - 3191
and
Propulsion Directorate
U.S. Army Aviation Systems Command
Cleveland, Ohio 44135 - 3191

10. Work Unit No.
505 -63-36
1L162211A47A

11. Contract or Grant No.

12. Sponsoring Agency Name and Address
National Aeronautics and Space Administration
Washington, D.C. 20546 - 0001
and
U.S. Army Aviation Systems Command
St. Louis, Mo. 63120 - 1798

13. Type of Report and Period Covered
Technical Memorandum

14. Sponsoring Agency Code

15. Supplementary Notes
Prepared for the 27th Joint Propulsion Conference cosponsored by AIAA, SAE, ASME, and ASEE, Sacramento, California, June 24-27, 1991. Paisan Somprakit and Ronald L. Huston, University of Cincinnati, Cincinnati, Ohio 45221; Fred B. Oswald, NASA Lewis Research Center. Responsible person, Fred B. Oswald, (216) 433-3957.

16. Abstract
This paper presents a new, innovative procedure called point load superposition for determining the contact stresses in mating gear teeth. It is believed that this procedure will greatly extend both the range of applicability and the accuracy of gear contact stress analyses. Point load superposition is based upon fundamental solutions from the theory of elasticity. It is an iterative numerical procedure which has distinct advantages over the classical Hertz method, the finite-element method (FEM), and over existing applications with the boundary element method (BEM). Specifically, friction and sliding effects, which are either excluded from or difficult to study with the classical methods, are routinely handled with the new procedure. The paper presents the basic theory and algorithms. Several examples are presented. Results are consistent with those of the classical theories. Applications with spur gears are discussed.

17. Key Words (Suggested by Author(s))	18. Distribution Statement
Contact stress Gear teeth Gears Numerical methods	Unclassified - Unlimited Subject Category 37

19. Security Classif. (of the report)	20. Security Classif. (of this page)	21. No. of pages	22. Price*
Unclassified	Unclassified	14	A03

NASA FORM 1626 OCT 86

*For sale by the National Technical Information Service, Springfield, Virginia 22161